

ornl

**OAK RIDGE
NATIONAL
LABORATORY**

MARTIN MARIETTA

OPERATED BY
MARTIN MARIETTA ENERGY SYSTEMS, INC.
FOR THE UNITED STATES
DEPARTMENT OF ENERGY

OAK RIDGE NATIONAL LABORATORY LIBRARIES



3 4456 0571533 0

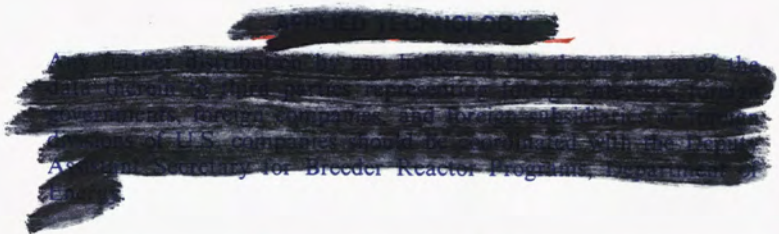
ORNL/TM-9211

Revised Analysis of the Transition Joint Life Test

W. K. Sartory

This document does not contain UCNI, ECI, or other unclassified sensitive information and has been approved for release to the public by:

David R. Hamrin 1/19/2010
David R. Hamrin, ORNL Classification Officer Date



OAK RIDGE NATIONAL LABORATORY

CENTRAL RESEARCH LIBRARY

CIRCULATION SECTION

4500N ROOM 175

LIBRARY LOAN COPY

DO NOT TRANSFER TO ANOTHER PERSON

If you wish someone else to see this report, send in name with report and the library will arrange a loan.

UCN-7969 13 9-77

Printed in the United States of America. Available from
the U.S. Department of Energy
Technical Information Center
P.O. Box 62, Oak Ridge, Tennessee 37830

This report was prepared as an account of work sponsored by an agency of the United States Government. Neither the United States Government nor any agency thereof, nor any of their employees, makes any warranty, express or implied, or assumes any legal liability or responsibility for the accuracy, completeness, or usefulness of any information, apparatus, product, or process disclosed, or represents that its use would not infringe privately owned rights. Reference herein to any specific commercial product, process, or service by trade name, trademark, manufacturer, or otherwise, does not necessarily constitute or imply its endorsement, recommendation, or favoring by the United States Government or any agency thereof. The views and opinions of authors expressed herein do not necessarily state or reflect those of the United States Government or any agency thereof.

ORNL/TM-9211
Dist. Category UC-79T,
-79Th, -79Tk, -79Tr

Engineering Technology Division

REVISED ANALYSIS OF THE TRANSITION JOINT LIFE TEST

W. K. Sartory

Date Published - July 1984

Prepared by the
OAK RIDGE NATIONAL LABORATORY
Oak Ridge, Tennessee 37831
operated by
MARTIN MARIETTA ENERGY SYSTEMS, INC.
for the
U.S. DEPARTMENT OF ENERGY
under Contract No. DE-AC05-84OR21400

CONTENTS

	<u>Page</u>
ABSTRACT	1
1. INTRODUCTION	1
2. SPECIMEN WELDMENT DESCRIPTION AND FINITE ELEMENT GRID	3
3. LOAD CONDITIONS	7
4. MATERIAL PROPERTIES	9
4.1 Thermal and Elastic Properties	9
4.2 Creep Equation	9
4.2.1 2 1/4 Cr-1 Mo steel base metal creep equation ...	9
4.2.2 2 1/4 Cr-1 Mo steel HAZ creep equation	9
4.2.3 ERNiCr-3 weld metal creep equation	11
4.2.4 Alloy 800H creep equation	11
4.3 Creep-Rupture Properties	12
4.4 Yield Stress	12
4.5 Plastic Modulus	13
5. THERMAL ANALYSIS PROCEDURES AND RESULTS	14
6. INELASTIC STRUCTURAL ANALYSIS PROCEDURES	17
7. ANALYTICAL RESULTS AND COMPARISON WITH EXPERIMENT	20
8. DISCUSSION OF RESULTS	28
9. SUMMARY	32
ACKNOWLEDGMENTS	33
REFERENCES	34



REVISED ANALYSIS OF THE TRANSITION JOINT LIFE TEST*

W. K. Sartory

ABSTRACT

The Transition Joint Life Test was performed by General Electric and the Energy Technology Engineering Center and was analyzed earlier by General Electric. Because of later developments in analysis techniques and in our understanding of the stress behavior near a dissimilar metal weldment, agreement was reached between General Electric and Oak Ridge National Laboratory's High-Temperature Structural Design program that a more up-to-date analysis was needed. This report presents results of a new analysis incorporating modified mechanical properties, revised constitutive equations, and a more refined finite element grid. The structural life prediction of the present report is quite conservative (~3 cycles of predicted life compared to 12 to 25 cycles of measured life), whereas the earlier General Electric analysis was underconservative by a similar factor.

Keywords: transition joint, dissimilar metal weldment, structural failure, thermal transients, ratchetting, creep-fatigue damage, inelastic analysis, piping

1. INTRODUCTION

Electrical power plants sometimes include both austenitic stainless steel and ferritic steel piping. The transition joints that couple the dissimilar metals have posed a reliability problem for fossil-fueled power plants and pose a potential reliability problem for liquid-metal-cooled fast breeder reactor (LMFBR) plants. In 1974, General Electric (GE) undertook a program involving both testing and analysis to improve the joints. The most detailed analysis was performed by Yang and Palmer¹ before any testing was carried out and was eventually found to be nonconservative by a factor of about 5. Following the Yang and Palmer analysis, additional information on the mechanical properties of transition joint

*Work performed under DOE/BTP AF 15 40 10 3, Task No. OR-1.1, High-Temperature Structural Design Technology.

life test (TJLT) materials was obtained, changes were made in the recommended constitutive equations, improved creep-rupture criteria were developed, and a study was performed on the effect of grid refinement near a dissimilar metal weldment. As a result, there has been some interest in the effect of these changes on the TJLT life prediction.

The Weldment Design Methodology subtask of the ORNL High-Temperature Structural Design program includes analytically assessing the deformation and failure behavior of structural weldments. The present revised analysis of the TJLT was performed under that subtask to contribute to our understanding of the adequacy of current design methodology as applied to transition joints.

2. SPECIMEN WELDMENT DESCRIPTION AND FINITE ELEMENT GRID

Each TJLT specimen² was a 0.457-m-OD (18-in.) pipe with a 25.4-mm (1.00-in.) wall incorporating three different base metals, two different weldment filler metals, and five different dissimilar metal circumferential weldments spaced far enough apart to avoid structural interactions (Fig. 1). Only one weldment involving 2 1/4 Cr-1 Mo steel and Alloy 800H base metals and ERNiCr-3 weld metal (Fig. 2) is analyzed in this report. The finite element grid is shown in Figs. 3 and 4.

Although the portion of the structure analyzed comprised only three different alloys, the analysis also incorporated a fourth material — the heat-affected zone (HAZ) of the 2 1/4 Cr-1 Mo steel, which was taken to have different mechanical properties from the 2 1/4 Cr-1 Mo steel base metal. Based on a recommendation of McAfee et al.,³ the HAZ was assumed to have a thickness of 1 mm (0.040 in.). The grid extended far enough on both sides of the weldment to minimize structural end effects. The end boundary conditions applied an axial load and permitted axial deflection but prevented rotation.

It is evident from Fig. 3 that the finite element grid is more highly refined in the neighborhood of the intersection between the ERNiCr-3/HAZ

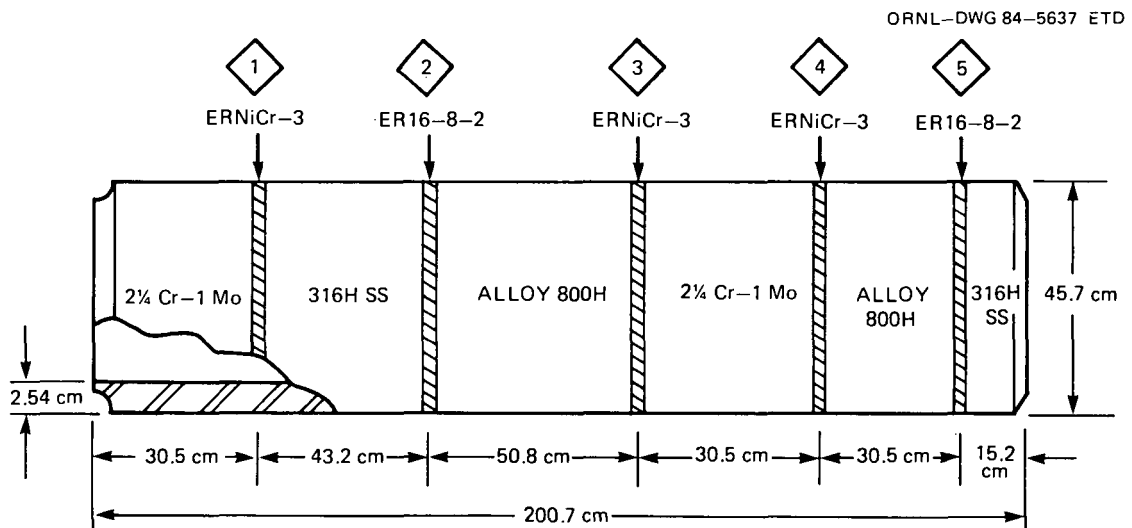


Fig. 1. TJLT Spool Assembly. Only weldment 4 is analyzed in this report. 1 in. = 2.54 cm.

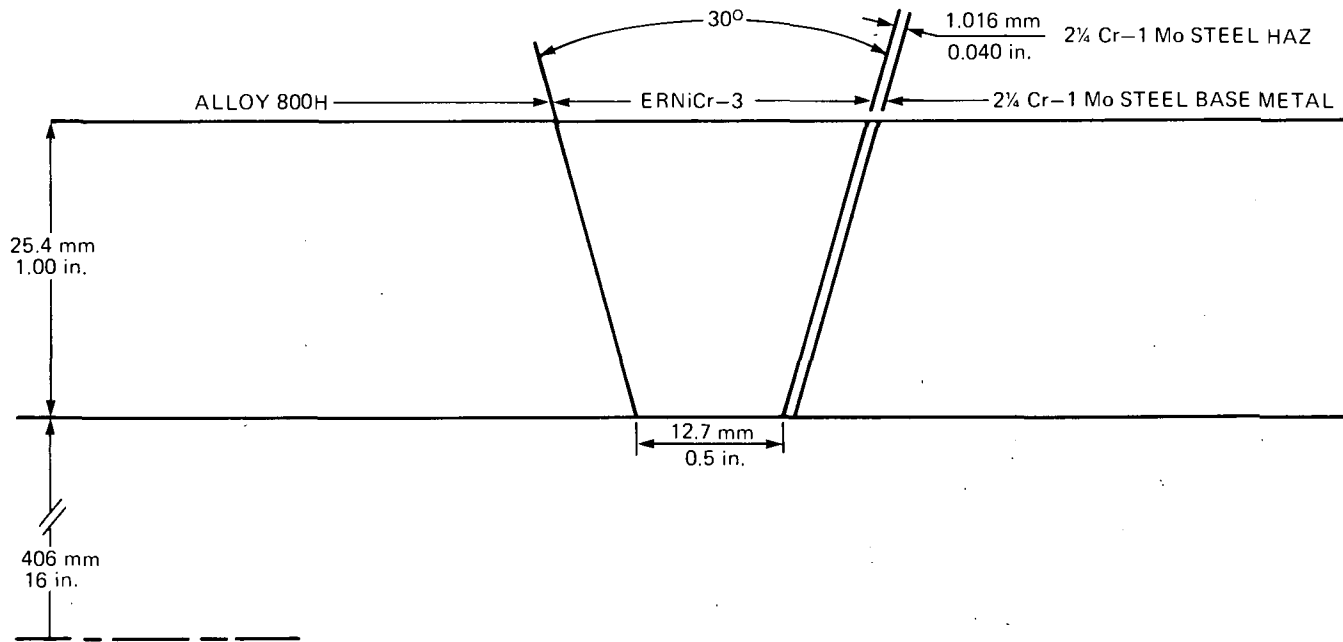
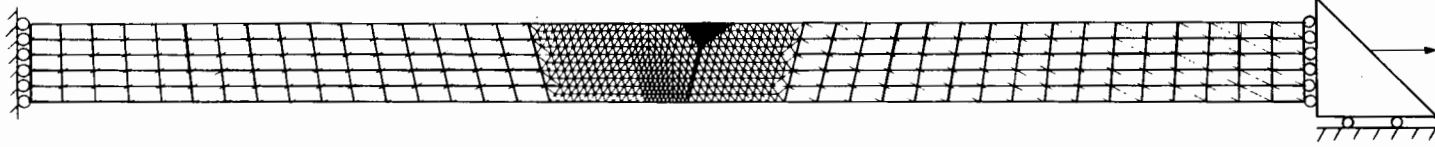
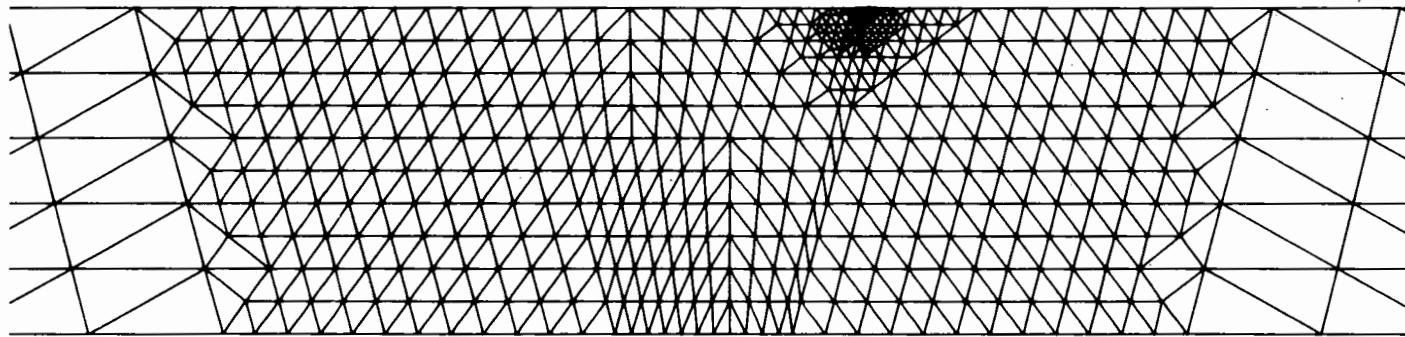


Fig. 2. Dissimilar metal weldment geometry and material zones.
Coolant flow direction is from left to right.



(a)



(b)

Fig. 3. Structural finite element grid. (a) Complete grid of 1298 elements showing end conditions. (b) Expanded view of weldment showing material zones.

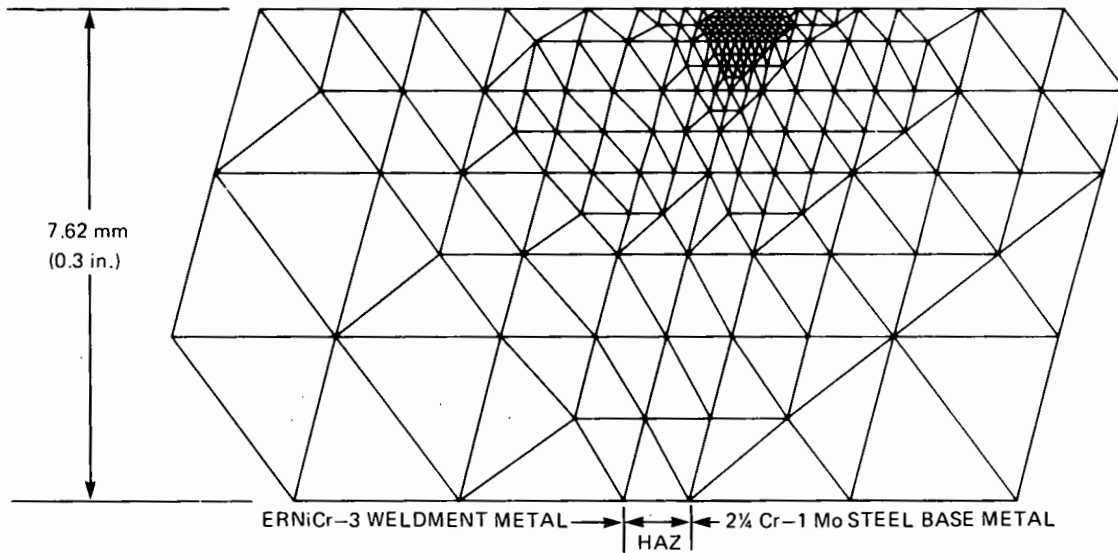


Fig. 4. Expanded view of the finite element grid refinement region. There are 328 elements in this region.

boundary and the outer surface of the pipe. There are two reasons for this refinement: (1) it is known from practical experience with transition joints as well as from the TJLT tests that initial failure occurs near the intersection, and (2) earlier analytical studies⁴ suggest a stress singularity at the intersection.

3. LOAD CONDITIONS

One of the difficulties in analyzing a weldment is determining suitable initial conditions. The present specimen was subjected to a postweld heat treatment for 1 h at 727°C (1340°F). For the analysis, the postweld heat treatment was assumed to leave the specimen in a stress-free state at 727°C (1340°F). All stresses and strains were assumed to be zero, and the geometry was assumed to be a perfect cylinder with the specimen depressurized at 727°C (1340°F).

Before the first thermal downshock was performed in the test, a series of thermal and mechanical load cycles was carried out to condition the strain gages. These cycles involved (1) cooling the specimen from 727°C (1340°F) to room temperature (RT), (2) slow thermal cycling between RT and 593°C (1100°F), and (3) axial load cycling between 0 and 1.779 MN (400 kips) and between 0 and 3.114 MN (700 kips) at both RT and 593°C (1100°F). In the analysis, although no attempt was made to follow the exact number and sequence of the pretest cycles, one cycle of each type was performed to place the specimen in the proper initial elastic-plastic state. Then the specimen was slowly heated from RT to 593°C (1100°F), an axial load of 1.779 MN (400 kips) was applied, and the first thermal downshock was begun.

Two types of thermal downshock were applied in the TJLT experiments. The downramp rate was nominally 5.6°C/s (10°F/s) for the mild downramp and 11.2°C/s (20°F/s) for the severe downramp. The previous analysis of Yang and Palmer¹ used the mild downramp but the present analyses used the severe downramp that was applied throughout the test of specimen No. 1 and during the initial testing phase of specimen No. 2.

In the tests and in the present analysis, after the thermal downramp was completed, the specimen was reheated slowly to 593°C (1100°F) and held at that temperature for 66 h at full 1.779-MN (400-kips) axial load while creep occurred. Then the next downramp was applied.

In the test, the axial load was removed occasionally and the specimen was slowly cooled to RT for inspection. In the present analysis, the load was never removed, and the specimen was never cooled to RT after the first downramp. The analytical load history is shown in Fig. 5.

ORNL-DWG 84-5641 ETD

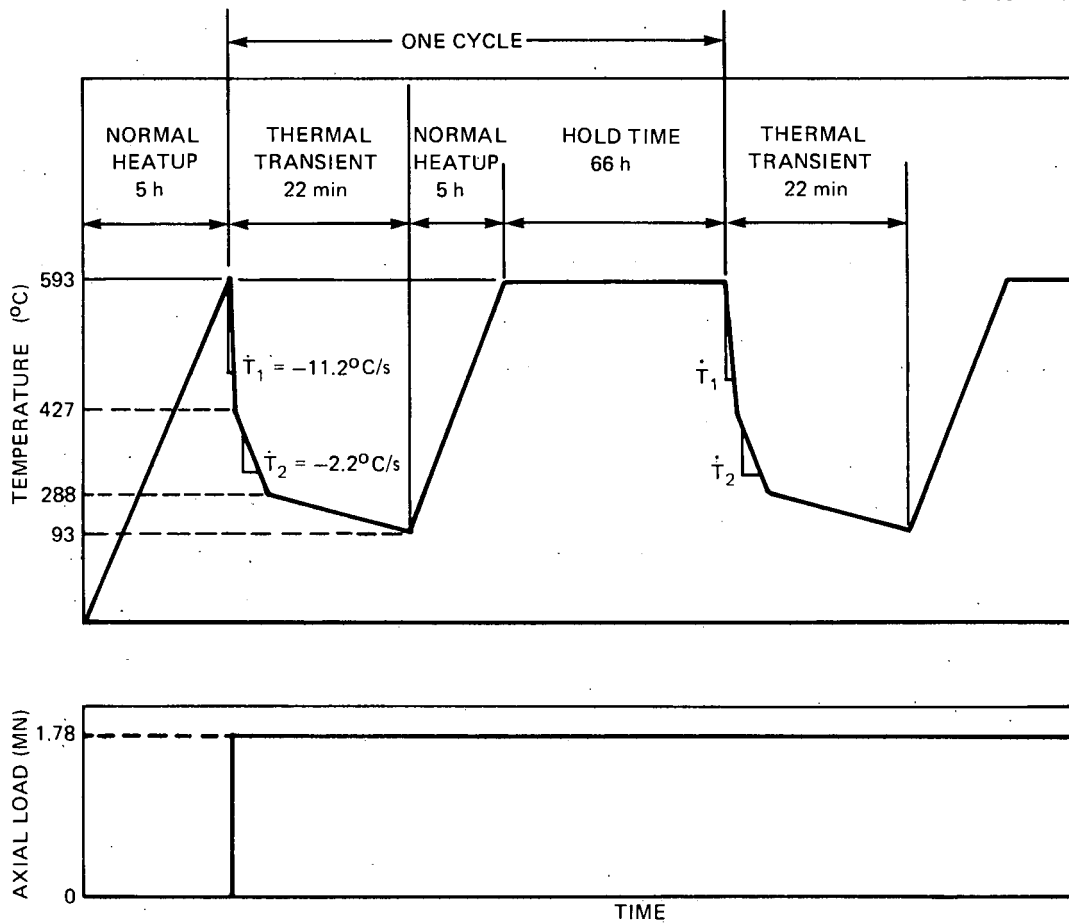


Fig. 5. Diagram of TJLT conditions showing nominal thermal downramp. The actual metal inner surface temperature is more complicated than the simple piecewise linear form shown on this schematic diagram. $1^\circ\text{C} = 1.8^\circ\text{F}$; $1 \text{ MN} = 225 \text{ kips}$.

4. MATERIAL PROPERTIES

4.1 Thermal and Elastic Properties

The thermal and elastic properties of 2 1/4 Cr-1 Mo steel, Alloy 800H, ERNiCr-3 weld metal, carbon steel (used for the centerbody), and nitrogen (the coolant) were obtained from various sources and fitted to least-squares polynomials in temperature as presented in Table 1.

4.2 Creep Equation

McAfee et al.³ performed a few additional creep tests of samples from a TJLT weldment ring and, based on the results, recommended creep equations to be used in the present analysis.

4.2.1 2 1/4 Cr-1 Mo steel base metal creep equation

For the 2 1/4 Cr-1 Mo steel base metal, the *Nuclear Systems Materials Handbook*⁵ equation was used with an ultimate tensile strength parameter of 305.5 MPa (44.3 ksi) as recommended by McAfee et al.³

4.2.2 2 1/4 Cr-1 Mo steel HAZ creep equation

For the 2 1/4 Cr-1 Mo steel HAZ, McAfee et al.³ recommended that the equations and data be re-examined. Based on only two creep curves measured with normalized and tempered material at 593°C (1100°F) and 100 and 155 MPa (14.5 and 22.5 ksi), respectively, a new equation was fit by least squares to obtain:

$$\epsilon^c = \frac{Cpt}{1 + pt} + \dot{\epsilon}_m t ,$$

where

$$C = 10^{(-2.06653 + 0.764960 \log_{10}\sigma)};$$

$$p = 10^{(-8.94363 + 3.79156 \log_{10}\sigma)};$$

$$\dot{\epsilon}_m = 10^{(-13.7233 + 5.24422 \log_{10}\sigma)};$$

ϵ^c = creep strain, %;

t = time, h;

σ = stress, MPa (1 MPa = 0.145 ksi).

Table 1. Thermal and elastic properties^a of TJLT materials

Property	Symbol	Material	Coefficient of power of T					Source	
			T ⁰	T ¹	T ²	T ³	T ⁴		T ⁵
Thermal expansion ^b	$\ln(\ell/\ell_0)$	2 1/4 Cr-1 Mo	0.	0.614909×10^{-5}	0.217533×10^{-8}	$-0.623780 \times 10^{-12}$			ASME ⁶
Young's modulus	E	2 1/4 Cr-1 Mo	0.309720×10^8	-0.591580×10^4	0.225475×10^1	-0.268175×10^{-2}			ASME ⁶
Poisson's ratio	ν	2 1/4 Cr-1 Mo	0.254	0.154×10^{-3}	-0.126×10^{-6}				NSMH ⁵
Thermal conductivity	k	2 1/4 Cr-1 Mo	0.170369×10^1	0.646639×10^{-3}	-0.136303×10^{-5}	0.908054×10^{-9}	$-0.356050 \times 10^{-12}$	0.611225×10^{-16}	NSMH ⁵
Volumetric heat capacity	ρg	2 1/4 Cr-1 Mo	0.297074×10^{-1}	0.807612×10^{-5}	0.246302×10^{-7}	$-0.399890 \times 10^{-10}$	0.234064×10^{-13}		NSMH ⁵
Thermal expansion	$\ln(\ell/\ell_0)$	Alloy 800H	0.	0.709001×10^{-5}	0.550265×10^{-8}	-0.78128×10^{-11}	0.556507×10^{-14}	$-0.135210 \times 10^{-17}$	ASME ⁶
Young's modulus	E	Alloy 800H	0.286182×10^8	-0.316966×10^4	-0.115501×10^1				ASME ⁶
Poisson's ratio	ν	Alloy 800H	0.332072×10^0	0.721963×10^{-4}	-0.691618×10^{-7}	0.333395×10^{-10}			Yang and Palmer ¹
Thermal conductivity	k	Alloy 800H	0.531560	0.440375×10^{-3}					Yang and Palmer ¹
Volumetric heat capacity	ρCp	Alloy 800H	0.348923×10^{-1}	-0.133352×10^{-5}	0.249120×10^{-9}				Yang and Palmer ¹
Thermal expansion	$\ln(\ell/\ell_0)$	ERNiCr-3	0.	0.675113×10^{-5}	0.308443×10^{-8}	$-0.261170 \times 10^{-11}$	0.108939×10^{-14}		Yang and Palmer ¹
Young's modulus	E	ERNiCr-3	0.285893×10^8	-0.101035×10^4	-0.289616×10^1				G.E. MARC output ⁷
Poisson's ratio	ν	ERNiCr-3	0.262018	0.565259×10^{-4}					Yang and Palmer ¹
Thermal conductivity	k	ERNiCr-3	0.688350	0.361509×10^{-3}	0.490290×10^{-7}				C. Yang ⁸
Volumetric heat capacity	ρCp	ERNiCr-3	0.311515×10^{-1}	0.120726×10^{-4}	-0.101547×10^{-7}	0.572581×10^{-11}			Yang and Palmer ¹
Thermal conductivity	k	Carbon steel	0.251019×10^1	-0.221639×10^{-3}	-0.831207×10^{-6}	0.301386×10^{-9}			NSMH ⁶
Volumetric heat capacity	ρCp	Carbon steel	0.274585×10^{-1}	0.344540×10^{-4}	-0.415233×10^{-7}	0.264235×10^{-10}			NSMH ⁶
Thermal conductivity	k	Nitrogen	0.109024×10^{-2}	0.198991×10^{-5}	-0.602150×10^{-9}	0.151105×10^{-12}			NSMH ⁶
Viscosity	μ	Nitrogen	0.317249×10^{-2}	0.553169×10^{-5}	-0.241541×10^{-8}	0.112726×10^{-11}	$-0.254540 \times 10^{-15}$		NSMH ⁶
Specific heat capacity	Cp	Nitrogen	0.249072	-0.913119×10^{-5}	0.444823×10^{-7}	$-0.155560 \times 10^{-10}$			NSMH ⁶

^aThe equations of this table are in English engineering units. In particular,

T is in °F; $T(^{\circ}\text{C}) = [T(^{\circ}\text{F}) - 32]/1.8$

ℓ_0 is the length of a specimen at -17.8°C (0°F) } any consistent units
 ℓ is the length of a specimen at temperature T }

E is in psi; 1 psi = 6.894757×10^{-3} MPa

ν is dimensionless

k is in Btu/h in. °F; 1 Btu/h in. °F = 20.75 W/m K

ρCp is in Btu/in.³ °F; 1 Btu/in.³ °F = 115.8 MJ/m³ K

μ is in lbm/in. h; 1 lbm/in. h = 4.961×10^{-3} Pa s

Cp is in Btu/lbm °F; 1 Btu/lbm °F = 4184 J/kg K

^bThe usual instantaneous thermal expansion coefficient is related to the quantity $\ln(\ell/\ell_0)$ given in this table by $\alpha = d[\ln(\ell/\ell_0)]/dT$.

4.2.3 ERNiCr-3 weld metal creep equation

For the ERNiCr-3 weld metal, following the recommendation of McAfee et al., the Yang and Palmer equation was used:

$$\epsilon^c = A t^m \sigma^n e^{-KQ/(RT)},$$

where

$$A = 0.00216\%,$$

$$m = 0.25,$$

$$n = 4.0,$$

$$Q = 256.5 \text{ MJ/mol (61,300 kcal/mol)},$$

$$R = 8314.4 \text{ J/mol K (1.987 kcal/mol K)},$$

$$K = 0.3,$$

$$\sigma = \text{stress (ksi) (1 ksi = 6.894757 MPa)},$$

$$T = \text{temperature (K) (1 K = 1.8}^\circ\text{R)}.$$

4.2.4 Alloy 800H creep equation

For Alloy 800H, McAfee et al.³ recommended the Yang and Palmer⁹ equation:

$$\epsilon^c = \frac{Cpt}{1 + pt} + \dot{\epsilon}_m t,$$

where

$$\dot{\epsilon}_m = 10^{(28.8341 - 46,083.2/T + \frac{7,610.12}{T} \log_{10}\sigma)};$$

$$p = 19/t_1;$$

$$t_1 = 10^{(-35.51 + 45,276.9/T + 8.707 \log_{10}\sigma - \frac{12,976.7}{T} \log_{10}\sigma)};$$

$$C = \epsilon_2 - \dot{\epsilon}_m t_2;$$

$$\epsilon_2 = 10^{(7.2384 - 11,298.8/T + \frac{2,153.8}{T} \log_{10}\sigma)};$$

$$t_2 = 0.00135 \exp(5,483.2/T) t_r^{0.940}, \quad T \geq 866 \text{ K};$$

$$t_r = 10^{(-18.452 + 34,025.8/T - \frac{6,431.06}{T} \log_{10}\sigma)};$$

ϵ^c = creep strain, %;

T = temperature, K (1 K = 1.8°R);

σ = effective stress, MPa (1 MPa = 0.145 ksi).

In exercising the Alloy 800H equation, it was found to predict negative creep strain for some stresses at 593°C (1100°F). The negative prediction was prevented by replacing the equation for C given above by

$$C = \max (0., \epsilon_2 - \dot{\epsilon}_m t_2) .$$

4.3 Creep-Rupture Properties

For the creep rupture of 2 1/4 Cr-1 Mo steel base metal, 2 1/4 Cr-1 Mo steel HAZ and ERNiCr-3 weld metal in a uniaxial stress state at 593°C (1100°F), the following data were taken from Yang and Palmer¹ (Table 2). In applying the data, linear interpolation or linear extrapolation on a log-log scale was used.

Table 2. Creep-rupture data at 593°C (1100°F)

Time (h)	Stress-to-rupture (ksi) ^a		
	2 1/4 Cr-1 Mo base	2 1/4 Cr-1 Mo HAZ	ERNiCr-3
10 ²	17.5	22.29	54.5
10 ³		14.76	
10 ⁴	8.74	9.29	
10 ⁵		5.36	40.65

^a1 ksi = 6.894757 MPa.

For creep rupture of Alloy 800H, Table I-14.6C of ASME Code Case⁶ N-47-21 was used. Unlike the data of Table 2, the ASME creep rupture represents a minimum stress-to-rupture and incorporates some conservatism.

4.4 Yield Stress

Based on the data of McAfee et al.³ and of Yang and Palmer,¹ linear equations for yield stress as a function of temperature were developed:

$$2 \text{ 1/4 Cr-1 Mo steel base metal: } \sigma_y = 28,000 - 8.70 T,$$

$$2 \text{ 1/4 Cr-1 Mo steel HAZ: } \sigma_y = 59,500 - 27.7 T,$$

$$\text{Alloy 800H: } \sigma_y = 26,200 - 4.341 T,$$

$$\text{ERNiCr-3: } \sigma_y = 47,800 - 8.182 T,$$

where σ_y is the yield stress in psi (1 psi = 6.894757×10^{-3} MPa), and T is the temperature in °F [$T(^{\circ}\text{C}) = [T(^{\circ}\text{F}) - 32]/1.8$].

4.5 Plastic Modulus

Plasticity in the TJLT analysis is mainly thermal plasticity. The analysis of thermal plasticity has recently been studied by Clinard.¹⁰ Based on the recommendation of Clinard, the plastic modulus in the present work was taken to be

$$E^P = -\frac{1}{\alpha} \frac{d\sigma_y}{dT} \text{ for the 2 1/4 Cr-1 Mo steel HAZ}$$

and

$$E^P = -\frac{1}{0.75 \alpha} \frac{d\sigma_y}{dT} \text{ for the other three metals .}$$

In the present work (unlike that of Clinard¹⁰), a temperature-dependent thermal expansion coefficient, α , is used, whereas $d\sigma_y/dT$ is constant. The use of a temperature-dependent E^P was not considered justified, therefore, in evaluating the equations for E^P , a constant value of α was calculated at 316°C (600°F), with the results as given in Table 3.

Table 3. Plastic modulus

Material	E^P
2 1/4 Cr-1 Mo HAZ	23.6 GPa (3.42×10^6 psi)
2 1/4 Cr-1 Mo base metal	9.86 GPa (1.43×10^6 psi)
Alloy 800H	4.34 GPa (0.629×10^6 psi)
ERNiCr-3	8.86 GPa (1.28×10^6 psi)

5. THERMAL ANALYSIS PROCEDURES AND RESULTS

Thermal analyses for the present work were performed using the finite element program CREEP-PLAST-HEAT.¹¹ The thermal finite element grid was identical to the structural grid shown in Fig. 3 except that the centerbody [a concentric 380-mm-OD (14.95-in.) carbon steel shell with a 4.76-mm wall (0.1875-in.)] was included in the thermal analysis. The nitrogen coolant stream that flowed between the specimen and the centerbody was modeled with finite differences to calculate the axial temperature distribution. Heat transfer between the coolant and the metal surfaces was represented by the equation recommended by McAdams.¹² The coolant inlet temperature and mass flow histories were obtained from Table 4. The outer surface of the specimen and the inner surface of the centerbody were assumed to be insulated.

The most important result of the thermal analysis (so far as the structural effect is concerned) is the temperature differential across the specimen wall. Ring et al.² report temperature differential histories for three measured severe downramps in the 2 1/4 Cr-1 Mo steel base metal near the weldment that is analyzed in the present work. The initial thermal analysis predicted a temperature differential significantly smaller than reported by Ring et al.² The heat transfer coefficient calculated from the standard correlation was then multiplied by 1.25, and the analysis was repeated to obtain the comparison illustrated in Fig. 6. This comparison was considered satisfactory so the thermal results with the 1.25 factor were used in the structural analysis.

Table 4. Coolant mass flow and inlet temperature history used in the analysis

Time (h)	Mass flow rate ^a (lb/h)	Coolant inlet temperature ^b (°F)
0.0	0	140
0.0002778	5,400	138.6
0.0005556	10,800	137.6
0.0008333	16,200	136.4
0.0011111	21,600	135.3
0.0013889	27,000	134.4
0.0016667	32,400	133.5
0.0019444	37,800	132.6
0.0022222	43,200	131.5
0.0025	48,600	130.8
0.0027778	54,000	129.9
0.0030556	59,400	129.1
0.0033333	64,800	128.3
0.0036111	70,200	127.7
0.0038889	75,600	126.8
0.0041667	81,000	126.2
0.0044444	86,400	125.5
0.0047222	91,800	124.8
0.005	97,200	124.2
0.0052778	102,600	123.6
0.0055556	108,000	122.9
0.0058333	113,400	122.3
0.0061111	118,800	121.7
0.0063889	124,200	121.0
0.0066667	129,600	120.5
0.0069444	135,000	119.9
0.0072222	134,892	119.2
0.0075	134,802	118.7
0.0077778	134,712	118.1
0.0080556	134,622	117.3
0.0083333	134,532	117.0
0.0086111	134,442	116.2
0.0088889	134,351	114.8
0.0091667	134,262	112.5
0.0094444	134,172	109.0
0.0097222	134,082	104.5
0.01111	133,632	86.3
0.0125	133,182	74.0
0.01389	132,732	67.7
0.01528	132,282	62.2
0.01667	131,832	58.7
0.01806	131,382	55.8
0.01944	130,932	53.8
0.02083	130,482	51.5
0.02222	130,032	49.5
0.02361	129,582	48
0.025	113,400	47
0.02639	97,200	46
0.02778	81,000	45
0.03056	69,468	42
0.03333	59,185	40
0.03611	50,189	39
0.03889	42,479	38
0.04167	36,054	37
0.04444	30,915	36
0.04722	27,063	35
0.05	24,496	35
0.05278	23,215	35
0.05556	23,220	35

^a 1 lb = 0.454 kg.

^b $T(^{\circ}\text{C}) = [T(^{\circ}\text{F}) - 32]/1.8.$

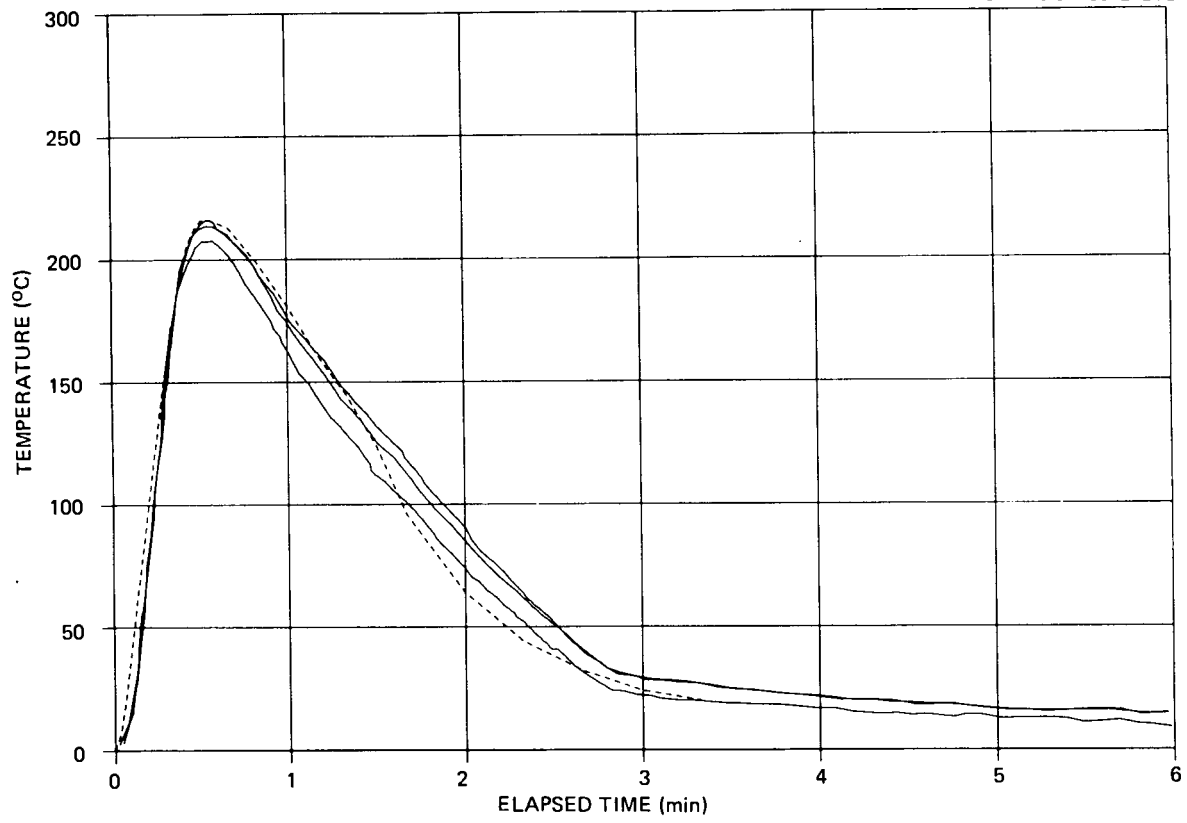


Fig. 6. Through-the-wall temperature differential during a thermal downramp. Solid curves - three selected experimental downramps. Dashed curve - calculated downramp.

6. INELASTIC STRUCTURAL ANALYSIS PROCEDURES

Structural analyses were performed using the finite element program PLACRE.¹³ The constitutive equations used (following Clinard¹⁰) were:

the yield condition:

$$\left[\frac{3}{2} (S_{ij} - \alpha_{ij})(S_{ij} - \alpha_{ij}) \right]^{1/2} = \sigma_y ;$$

the flow law:

$$d\epsilon_{ij}^P = \frac{1}{C\sigma_y} \left[\frac{3}{C\sigma_y} (S_{kl} - \alpha_{kl}) d\sigma_{kl} - MdT \right] (S_{ij} - \alpha_{ij}) ,$$

$$\text{with } C = \frac{2}{3} E^P ;$$

the growth law for α_{ij} :

$$d\alpha_{ij} = \frac{1}{\sigma_y} \left[\frac{3}{2\sigma_y} (S_{kl} - \alpha_{kl}) d\sigma_{kl} - NdP - MdT \right] (S_{ij} - \alpha_{ij}) ;$$

the growth law for σ_y :

$$d\sigma_y = NdP + MdT .$$

The variables are identified in the usual manner: $\sigma_y = \sqrt{3\kappa}$ is the bilinear uniaxial yield stress; $P = \int \sqrt{2/3} d\epsilon_{ij}^P d\epsilon_{ij}^P$ is the path length of plastic strain; T is the temperature; C is the bilinear plastic hardening coefficient; α_{ij} is the center of the yield surface; ϵ_{ij}^P is the plastic strain; σ_{ij} and S_{ij} are the stress and stress deviator, respectively; N and M are functions that specify the change of σ_y with change of path length and temperature, respectively.

In the present work, it was felt that the amount of data available did not justify the development of a law giving the effect of plastic strain dP on σ_y . Thus, N was set to zero; a fully hardened yield stress was used; and

$$d\sigma_y = MdT ,$$

where M was obtained by differentiating the equations for the material yield stress given earlier.

The maximum α -reset procedure¹⁴ was followed. That is, whenever elastic unloading occurred in an element, the value of α_{ij} was shifted toward the origin as far as possible (until $\alpha = 0$) consistent with the requirement that the current stress point must not fall outside of the yield surface.

Creep behavior was described in PLACRE by an equation-of-state formulation using strain hardening. The creep strain increment was given by

$$d\varepsilon_{ij}^C = \frac{3}{2} \frac{\dot{\varepsilon}^C(\bar{\sigma}, \bar{\varepsilon}^H)}{\bar{\sigma}} \sigma'_{ij} dt ,$$

where $\dot{\varepsilon}^C$ is the effective creep strain rate obtained from uniaxial data, $\bar{\sigma}$ is the effective stress,

$$\bar{\sigma} = \sqrt{\frac{3}{2} \sigma'_{ij} \sigma'_{ij}} ,$$

$\bar{\varepsilon}^H$ is a modified effective total* creep strain, and dt is the time increment. In the case of monotonic creep, $\bar{\varepsilon}^H$ is the effective total creep strain,

$$\bar{\varepsilon}^H = \sqrt{\frac{2}{3} \varepsilon_{ij}^C \varepsilon_{ij}^C} .$$

In the case of creep under cyclic loading, special rules have been established for determining $\bar{\varepsilon}^H$, based on the loading history.¹⁴ The cyclic creep rules of Ref. 14 were used in the present work.

The procedure that brings in an influence of reverse plastic strains on subsequent creep response predictions¹⁴ was used.

*Total creep strain means the sum of the primary and secondary creep strains. (Some strain-hardening procedures use only the primary creep strain for hardening.)

Creep-rupture damage was evaluated in the usual way by calculating the integral

$$\int_0^t \frac{dt}{T_d},$$

where t is time, and T_d is the creep-rupture time at the actual calculated Huddleston¹⁵ equivalent stress level.

Note that, for design purposes, the calculated stress is usually divided by a constant $K' < 1.0$ before evaluating the creep-rupture time T_d in order to ensure conservatism. Conservatism was not incorporated into this analysis. The damage integral was taken over the creep-hold periods only.

The Huddleston equivalent stress¹⁵ is given by

$$\sigma_e = \frac{3}{2} S_1 \left(\frac{2}{3} \frac{\bar{\sigma}}{S_1} \right)^{1.0} \exp \left[0.24 \left(\frac{J_1}{S_s} - 1 \right) \right],$$

where

$$J_1 = \sigma_1 + \sigma_2 + \sigma_3,$$

$$S_1 = \sigma_{\max} - J_1/3,$$

$$\bar{\sigma} = \sqrt{(\sigma_1 - \sigma_2)^2 + (\sigma_2 - \sigma_3)^2 + (\sigma_3 - \sigma_1)^2}/2},$$

$$S_s = \sqrt{\sigma_1^2 + \sigma_2^2 + \sigma_3^2},$$

$\sigma_1, \sigma_2, \sigma_3$ are the principal stresses,

$$\sigma_{\max} = \max(\sigma_1, \sigma_2, \sigma_3).$$

7. ANALYTICAL RESULTS AND COMPARISON WITH EXPERIMENT

The principal result of the present work is the prediction of time-to-failure. The calculated fatigue-damage fraction is less than about 0.1% of the creep damage and, following Yang and Palmer,¹ is not included in the life assessment. Analytical failure is taken to mean unit calculated creep damage and was reached during the third-cycle creep-hold period. Experimentally, failure is taken to mean the occurrence of the first observable crack and was reached some time between cycles 12 and 40 (out of 53 cycles performed) in TJLT specimen No. 1 and some time before cycle 25 (out of 25 severe cycles performed) in specimen No. 2. In the Yang and Palmer analysis¹ (which applied to a somewhat milder cycle than analyzed herein), predicted failure occurred in 158 cycles. Thus, the present analysis is significantly overconservative in predicting the allowable structure life whereas the Yang and Palmer analysis is underconservative.

One way to illustrate the significance of the discrepancy between calculated and measured failure time is to plot the probability density of the predicted failure. Creep-rupture tests, even the simplest constant-load isothermal uniaxial tests performed in the metallurgical laboratory, always show significant scatter; it is therefore reasonable to treat predicted failure in a statistical sense as was done earlier for test TT6.¹⁶ For the present analysis, we use the probability density curve adopted by Ring et al.² shifted to agree with the present prediction of failure at the third cycle (Fig. 7). Also shown on the figure is the experimental failure range taken for the purposes of illustration to be 12 to 25 cycles. (Failure was observed to occur some time between cycles 12 and 40 in specimen No. 1 and between cycles 1 and 25 in specimen No. 2. If we assume that failure occurred in the same cycle in the two duplicate tests, it must have occurred between cycles 12 and 25. If we do not make such an assumption, we can only say that both failures occurred between cycles 1 and 40, an interval that includes essentially the entire plot of Fig. 7.)

Figure 8 shows the calculated creep damage contours in and near the HAZ near the outer pipe radius at the end of the third cycle. The region

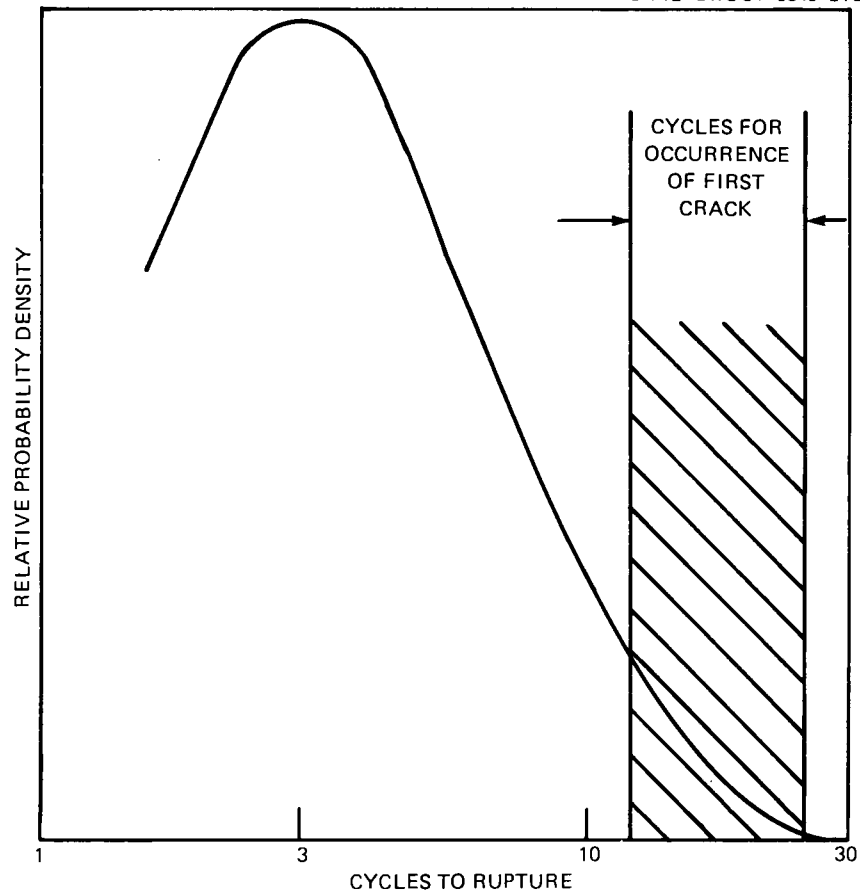


Fig. 7. Calculated probability density of predicted cycles-to-rupture compared to experimental range for crack initiation.

of unit creep damage extends about $220\ \mu\text{m}$ (9 mils) deep from the outer surface into the HAZ. The creep damage fraction in the 2 1/4 Cr-1 Mo steel base metal exceeds 0.1 but does not reach 0.2. By contrast, Yang and Palmer¹ calculated higher creep damage in the 2 1/4 Cr-1 Mo steel base metal than in the HAZ. The creep damage fraction is much less in the ERNiCr-3 weld metal and in the Alloy 800H (not shown) than in the 2 1/4 Cr-1 Mo steel. The calculated fatigue damage fraction is less than about 0.1% of the creep damage and, following Yang and Palmer, is not included in the present life assessment.

Figure 9 shows the Mises effective stress contours near the weldment at the beginning of the third creep-hold period. The highest effective stress occurs near the inner surface in the ERNiCr-3 weld metal. The

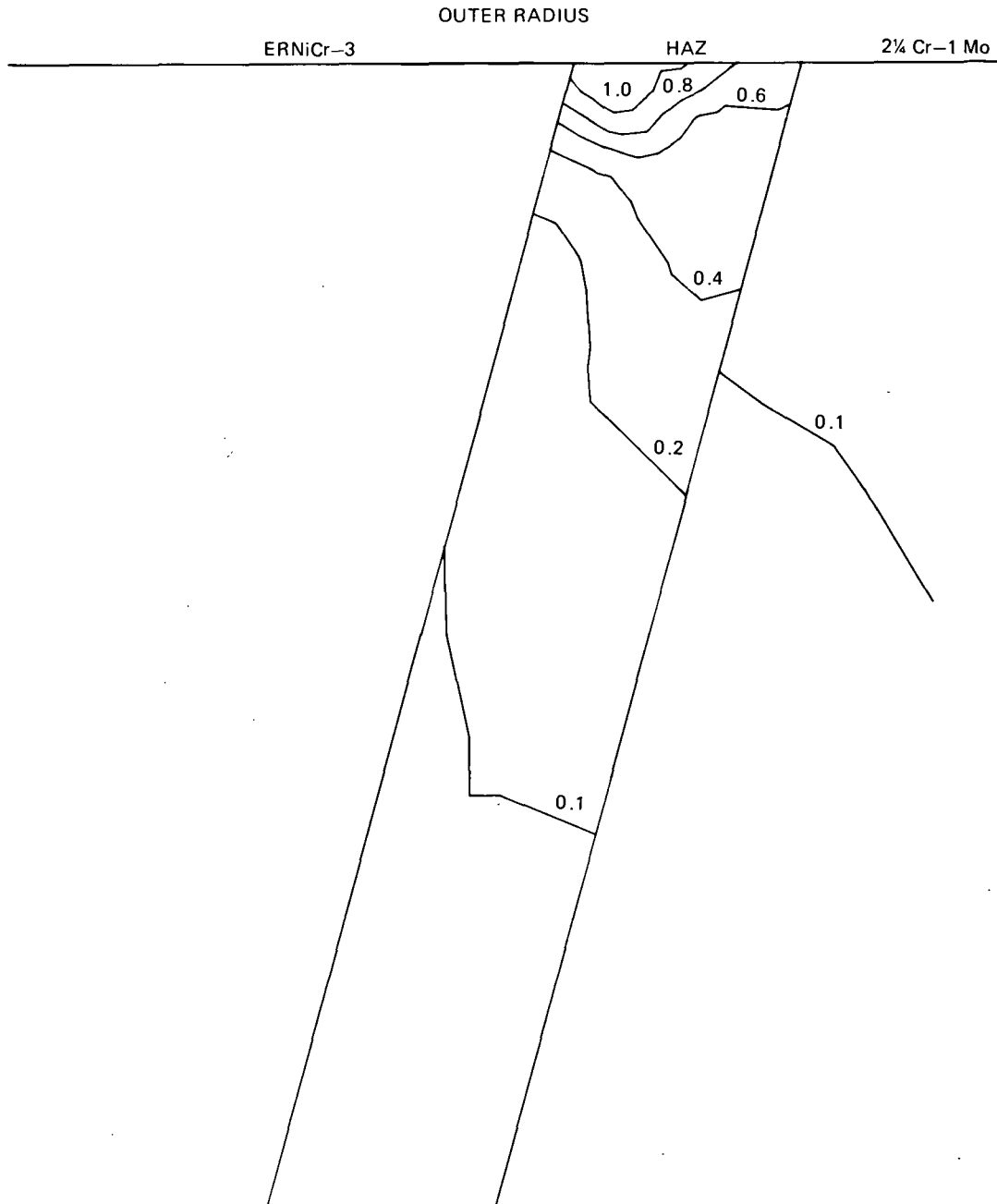


Fig. 8. Calculated creep damage fraction contours at end of third cycle.

highest stress in the HAZ also occurs near the inner surface of the pipe, but the inner surface HAZ stress decreases rapidly during the creep-hold period. The effective stress in the HAZ diminishes toward the interior of the wall and then increases again near the outer surface. The effective

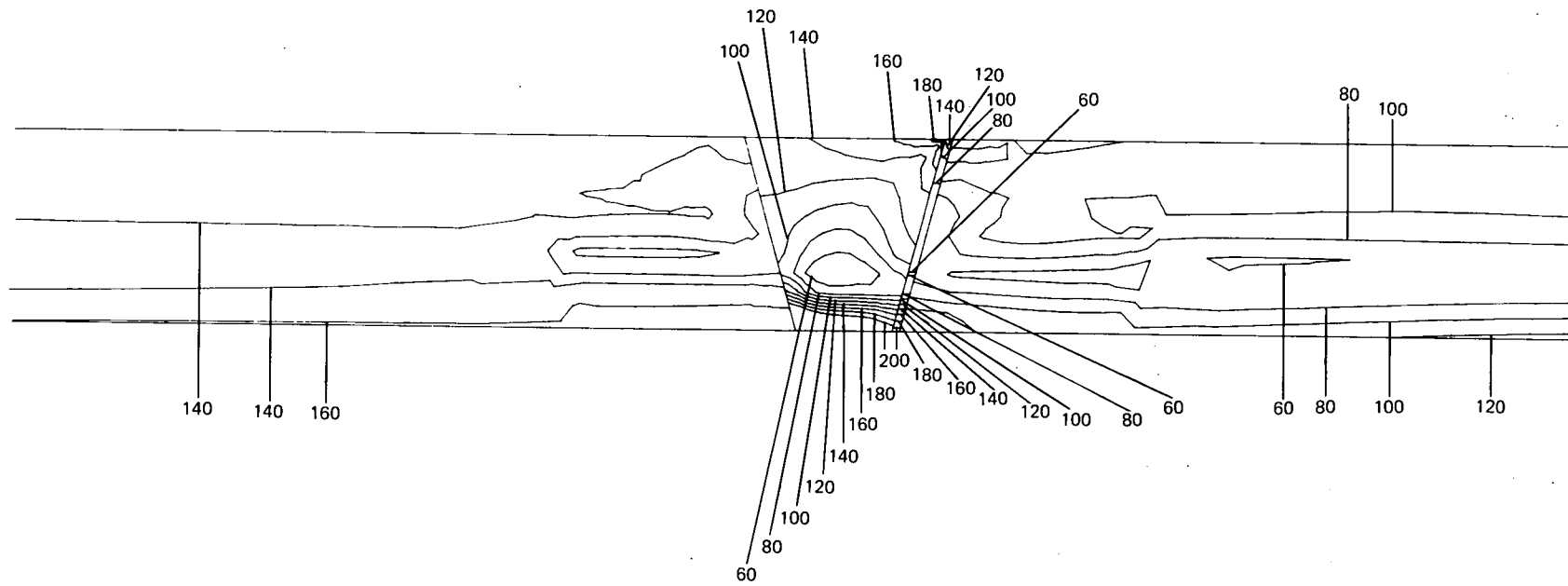


Fig. 9. Calculated contours of Mises effective stress at start of third creep hold period. The stresses are given in MPa. (1 MPa = 0.145 ksi.)

stress near the outer surface of the HAZ persists longer during the creep-hold periods and thus causes the greatest creep damage. (The creep damage reported herein was based on the Huddleston equivalent stress rather than the Mises effective stress, but the difference is minor for the conditions of the analysis.)

Figure 10 shows contours of the calculated effective creep strain at the end of the third cycle. The maximum effective creep strain occurs in the 2 1/4 Cr-1 Mo steel base metal near the outer surface of the pipe near the HAZ. The effective creep strain in the HAZ exceeds 0.0075 m/m near the outer surface of the pipe, but the contours in the HAZ are not clearly distinguishable on the scale of the figure.

Figure 11 shows contours of the calculated effective plastic strain at the end of the third cycle. The peak effective plastic strain occurs at the inner surface in all four metals, reaching 0.006 m/m in the 2 1/4 Cr-1 Mo steel base metal, 0.005 m/m in the HAZ, 0.003 m/m in the ERNiCr-3, and 0.003 m/m in the Alloy 800H. The plastic strain also increases near the outer surface near the HAZ but does not reach the inner surface value.

Comparison of the strains predicted in the present analysis with the strain measured and predicted by GE is also of interest. Ring et al.² do not present overall ratchetting strains, but they do present incremental strains during the creep-hold period of the second cycle. The most interesting of the creep strain results are those obtained by the axial gages designated C10 and C11 as presented in Table 5.

Table 5. Comparison of incremental strains^a
during the second creep period

Gage	Material	GE analysis	ORNL analysis	Experimental specimen	
				No. 1	No. 2
C10	2 1/4 Cr-1 Mo	115	736	520	560
C11	2 1/4 Cr-1 Mo	130	881	370	270

^aAll strains are in $\mu\text{m}/\text{m}$.

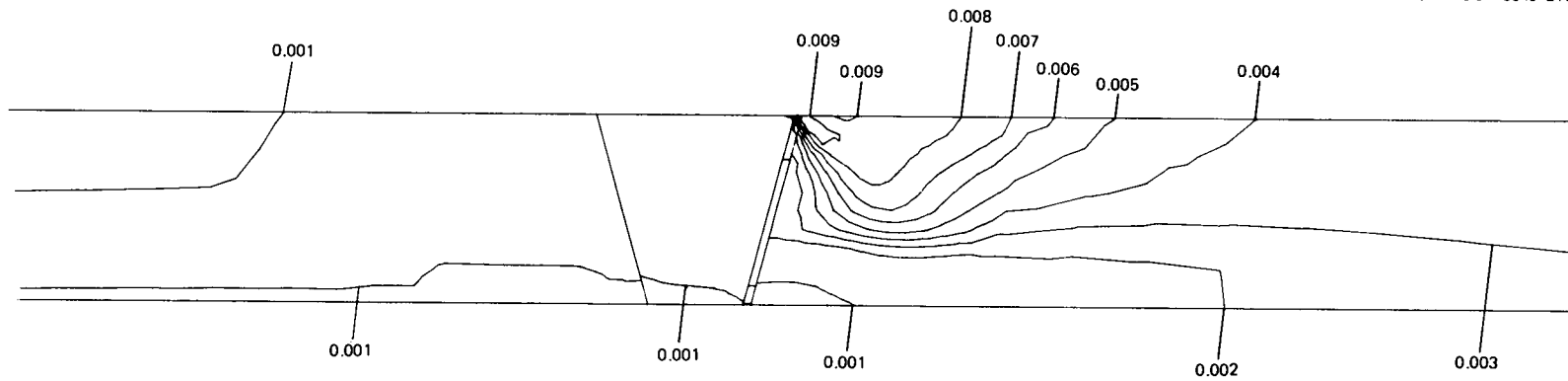


Fig. 10. Calculated contours of effective creep strain at end of third cycle. The strains are in m/m.

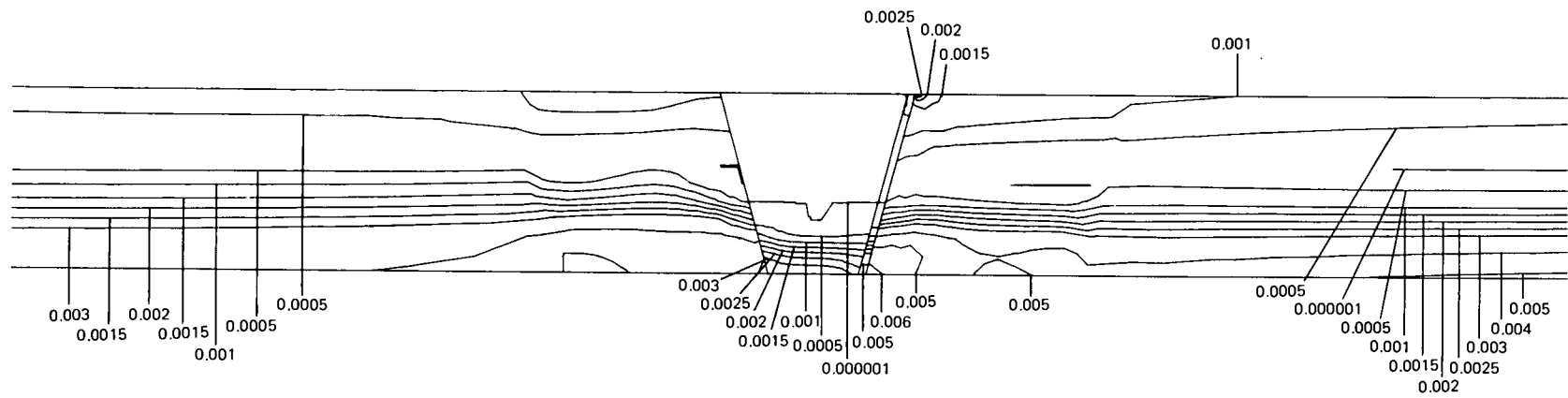


Fig. 11. Calculated contours of effective plastic strain at end of third cycle. The strains are in m/m.

The strains predicted by GE are significantly less than those of the present analyses, probably because of the milder thermal downramp applied and the difference in material properties used. The experimental results lie between the two calculations. Also notable is the result that, in both analyses, the strain is greater at gage C11 [~150 mm (6 in.) from the weldment] than in gage C10 [~75 mm (3 in.) from the weldment], whereas the measurements show the opposite trend.

8. DISCUSSION OF RESULTS

In this section, the discrepancies between the present work and the TJLT experiments² and between the present work and the analyses of Yang and Palmer¹ are discussed.

First, note that the magnitude of the difference between the present prediction of time-to-failure and the observed crack initiation in the TJLT experiments is comparable to the magnitude of the difference found in the earlier TT6 experiment,¹⁶ so such a discrepancy is not surprising. The analytical/experimental discrepancy in the ratchetting creep strain is also not out of line with earlier work.

On the other hand, specimen Nos. 1 and 2 provide two independent experiments that seem to give discrepancies relative to the analysis that are in the same direction and roughly of the same magnitude.* This consistency of the experimental results greatly reduces the plausibility of attributing the analytical/experimental discrepancy to the usual random scatter of creep-rupture experiments and is strong evidence that the discrepancy is due to uncertainties of assumptions and input for the analytical prediction procedure.

Although a few additional mechanical property measurements were made in preparation for the present analyses,³ the overall amount of heat-specific data available is less than in the earlier TTT test series.¹⁷⁻¹⁹ Property uncertainty, therefore, remains a significant source of error in the analyses.

The HAZ modeling problem also presents unusual difficulties. Although a single HAZ with a 1.02-mm (0.040-in.) thickness was adopted for the present analysis, it is possible that a multizone model²⁰ or even a continuous-property-variation model is needed for a satisfactory analysis.

The fusion boundary singularity problem also requires discussion. The fusion boundary between the ferritic 2 1/4 Cr-1 Mo steel and the austenitic ERNiCr-3 weld metal is expected to be quite sharp. In the region

*Since specimen No. 2 was already cracked at the first inspection, it cannot definitely be proven that it did not fail much earlier, but the small, measured crack depth at 25 cycles strongly suggests that it failed long after the 3-cycle prediction of the present analysis.

where the fusion boundary intersects the surface of the pipe, a stress singularity occurs⁴ that can give rise to infinite predicted stresses. The appropriate method of handling an infinite predicted stress in the current life prediction methodology is not clear. In the present work unbounded predicted stresses were avoided by deliberately limiting the smallest finite element to 0.13 mm (5 mils). This was done on the grounds that, although much smaller elements were likely to lead to prediction of even higher stresses, a high stress that was limited to a region smaller than 0.13 mm (5 mils) would not cause an observable crack. The adequacy of the 0.13-mm (5-mil) element size and even the appropriateness of resolving the stress singularity problem in this way are still open to question, however.

We now turn to discussion of the discrepancy between the present work and the Yang and Palmer analysis.¹ In some ways, this discrepancy could be more disturbing than the analytical/experimental difference because it is much larger and because, if various analysts cannot make consistent predictions, then there is no hope of predicting experimental behavior.

To elucidate the creep damage evaluations, we report some relevant calculated Mises effective stresses* in Table 6.

As a basis of comparison, line (1) of Table 6 gives the primary axial stress, which is the same in both analyses throughout the test. Line (2) (also included for reference purposes) indicates that at the outer surface during the third cycle of the present analyses in the region of the 2 1/4 Cr-1 Mo steel base metal, far from the weldment, the stress decays from 110 MPa (16 ksi) at the start of the creep-hold period to 55 MPa (7.9 ksi) at the end of the creep-hold period (i.e., the effective stress decays almost to the primary stress level). Line (3) shows the peak stress in the HAZ during the first cycle of the present analyses, and line (4) gives the same result for the Yang and Palmer analysis. At the start of the first creep-hold period, the calculated stresses are not too different, but the stress at the end of the first creep-hold period provides the

*Creep damage in the present work is based on the Huddleston equivalent stress rather than the Mises effective stress. Examination of the calculated stress tensors indicate that the difference is only about 10% of the effective stress. The calculated stress differences in Table 6 are much larger.

Table 6. Comparison of calculated effective stresses of the present analyses with those of Yang and Palmer

Quantity	Start of hold period [MPa (ksi)]	End of hold period [MPa (ksi)]
1. Primary axial stress	52 (7.5)	52 (7.5)
2. Outer surface effective stress at third cycle far from weldment (present work)	110 (16)	55 (7.9)
3. Peak HAZ effective stress in first cycle (present work)	159 (23)	104 (15.1)
4. Peak HAZ effective stress in first cycle (Yang and Palmer)	148 (21.5)	43 (6.3)
5. Peak HAZ effective stress in third cycle (present work)	141 (20.5)	128 (18.6)
6. Peak HAZ ^a effective stress in fourth cycle (Yang and Palmer)	37 (5.4)	34 (4.9)

^aYang and Palmer report higher stresses and more creep damage in the 2 1/4 Cr-1 Mo steel base metal near the HAZ than in the HAZ itself.

first major discrepancy. The stress calculated in the present work decays less in the HAZ than in the region far from the weldment reported in line (2), whereas the stress calculated by Yang and Palmer decays even below the primary stress. Two possible reasons are suggested for this difference: (1) the HAZ creep equation used in the present work (and the experimental creep curves on which it was based) indicates a smaller creep rate than the equation used in the Yang and Palmer analysis; and (2) it is believed that with the more highly refined grid used in the present analyses, a significant amount of elastic follow-up occurs near the stress singularity. That is, as creep redistribution of stress occurs, elastic energy flows toward the singularity from the surrounding stressed material and retards the rate of stress decay.

Lines (5) and (6) of Table 6 present calculated stresses during the third and fourth cycles* and indicate an even more remarkable difference

*Different cycles are compared here because of the availability of results.

between the analyses. The stress calculated in the present work is significantly (but not totally) rejuvenated with each new downramp and decays less during the third cycle than during the first cycle (presumably due to creep hardening). The Yang and Palmer analysis, on the other hand, begins the fourth creep-hold period with a stress even lower than the primary stress and predicts that the stress decays even further during the redistribution of the creep-hold period. Two reasons are suggested for the difference in the degree of stress rejuvenation during each downramp: (1) the α -reset procedure used in the present work but not by Yang and Palmer is expected to promote stress rejuvenation; and (2) the difference in the magnitude of the thermal downshock rate could also be important.

Finally, note that there are many differences in the analyses, and the differences in input most likely to be responsible for the discrepancies in results have been cited here. Only a detailed sensitivity study in which the differences in input between the two analyses are removed, one-by-one, could establish definitely which are most important.

9. SUMMARY

An Alloy 800H-ERNiCr-3-2 1/4 Cr-1 Mo steel dissimilar metal weldment that was a part of the TJLT specimens is re-analyzed using modified mechanical properties, more up-to-date constitutive equations, and a finite element grid that is highly refined in the region where failure is expected. The predicted time-to-failure is less than 3 cycles compared to a measured life of 12 to 40 cycles for TJLT specimen No. 1 and less than 25 cycles for specimen No. 2. In the present report, predicted structural failure is identified with the calculation of unit creep damage in some finite element and is directly compared to the appearance of the first observable cracking in the experiment. Actually, the precise experimental significance to be attached to a unit calculated damage fraction in a complicated structure with stress gradients is not definitely established. The occurrence of a significant factor of conservatism between unit damage and the first observed cracking might be regarded as reassuring. The calculated incremental axial strain occurring during the second creep-hold period is compared to experiment and is also found to be conservative. Possible reasons for the discrepancy between the present work and the TJLT experiment and between the present work and the previous analyses of Yang and Palmer are discussed.

ACKNOWLEDGMENTS

The author would like to thank the many staff members of ORNL, GE, and ETEC who contributed to the work. C. E. Pugh, A. W. Dalcher, and J. M. Corum pointed out the need for the present analyses. W. J. McAfee directed this activity during its early stages and, along with R. W. Swindeman and B. C. Williams, developed many of the mechanical property correlations used. J. A. Clinard and R. L. Huddleston provided advice concerning the thermal plasticity modeling and creep-rupture criterion, respectively. H. J. Busboom, C. C. Yang, R. C. Soucy, and W. Bowers provided information about the TJLT experiments and the previous analyses. J. A. Clinard and R. C. Gwaltney reviewed the report.

REFERENCES

1. T. M. Yang and W. R. Palmer, *Inelastic Stress Analysis of 2 1/4 Cr-1 Mo to Alloy 800H Pipe Joint of TJLT Article No. 1*, GEFR-00453, General Electric Company (May 1979).
2. P. J. Ring et al., *Transition Joint Development Program - Final Report*, GEFR-00645, General Electric Company (December 1982).
3. W. J. McAfee et al., "Property characterizations," pp. 4-98 to 4-107 in *High-Temperature Structural Design Technology Program Semiannual Progress Report for Period Ending June 30, 1983*, ORNL/MSP/1.1-83/3, Union Carbide Corp. Nuclear Div., Oak Ridge Natl. Lab.
4. J. A. Clinard and W. K. Sartory, "Analyses of a thick-wall pipe (reference problem)," pp. 4-109 to 4-114 in *High-Temperature Structural Design Technology Program Semiannual Progress Report for Period Ending June 30, 1983*, ORNL/MSP/1.1-83/3, Union Carbide Corp. Nuclear Div., Oak Ridge Natl. Lab.
5. U.S. Department of Energy, *Nuclear Systems Materials Handbook*, Hanford Engineering Development Laboratory, Richland, Washington.
6. ASME Code Case N-47-21, *Cases of ASME Boiler and Pressure Vessel Code*, American Society of Mechanical Engineers, New York, 1981.
7. C. C. Yang, General Electric, personal communication to W. K. Sartory, Oak Ridge National Laboratory, September 10, 1981.
8. C. C. Yang to A. W. Dalcher, General Electric Internal Memo YL-600-20049, March 25, 1982.
9. T. M. Yang and W. R. Palmer, *Preliminary Material Properties for Inelastic Analyses of TJLT Articles*, GEFR-00460, General Electric Company, April 1978.
10. J. A. Clinard, "Development of Modifications to NE F 9-5T Constitutive Equation Guidelines," pp. 4-4 to 4-18 in *High-Temperature Structural Design Technology Program Semiannual Progress Report for Period Ending June 30, 1983*, ORNL/MSP/1.1-83/3, Union Carbide Corp. Nuclear Div. Oak Ridge Natl. Lab.
11. Y. R. Rashid, *Part II: User's Manual for CREEP-PLAST Computer Program*, GEAP-13262-1, General Electric Company, March 1973.
12. W. H. McAdams, *Heat Transmission*, 3rd ed., McGraw-Hill, New York, 1954, p. 242.
13. W. K. Sartory, *PLACRE User's Manual*, ORNL/TM-5626, Union Carbide Corp. Nuclear Div., Oak Ridge Natl. Lab., February 1977.

14. *Guidelines and Procedures for Design of Class I Elevated Temperature Nuclear System Components*, NE Standard F9-5T, Department of Energy, March 1981.
15. R. L. Huddleston, "Strength theory assessments and development," pp. 4-27 to 4-39 in *High-Temperature Structural Design Technology Program Semiannual Progress Report for Period Ending December 31, 1983*, ORNL/MSP/1.1-84/1, Union Carbide Corp. Nuclear Div., Oak Ridge Natl. Lab.
16. W. K. Sartory et al., *Thermal Ratchetting Test to Rupture of Type 304 Stainless Steel Pipe: Test TT-6*, ORNL-5890, Union Carbide Corp. Nuclear Div., Oak Ridge Natl. Lab., September 1982.
17. J. M. Corum et al., *Thermal Ratchetting Tests of Type 304 Stainless Steel Pipe: Specimen TTT-1 and TTT-2*, ORNL-5386, Union Carbide Corp. Nuclear Div., Oak Ridge Natl. Lab., June 1978.
18. W. K. Sartory et al., *Thermal Ratchetting Test of 2 1/4 Cr-1 Mo Steel to Type 316 Stainless Steel Pipe: Test TTT-3*, ORNL-5330, Union Carbide Corp. Nuclear Div., Oak Ridge Natl. Lab., October 1977.
19. W. K. Sartory et al., *Thermal Ratchetting Test of Type 316 Stainless Steel Seamless to Seam-Welded Pipe: Specimen TTT-4*, ORNL-5430, Union Carbide Corp. Nuclear Div., Oak Ridge Natl. Lab., September 1978.
20. W. J. McAfee, R. L. Battiste, and R. W. Swindeman, *Elevated Temperature (593°C) Tests and Analyses of Type 304/308-CRE Stainless Steel Plate Weldments*, ORNL/TM-9065, Union Carbide Corp. Nuclear Div., Oak Ridge Natl. Lab., May 1984.

6

ORNL/TM-9211

Dist. Category UC-79T,
-79Th, -79Tk, -79TrInternal Distribution

- | | |
|-------------------------------|--------------------------------------|
| 1. R. L. Battiste | 18. H. C. McCurdy |
| 2. J. J. Blass | 19. J. G. Merkle |
| 3. C. R. Brinkman | 20. S. E. Moore |
| 4. J. A. Clinard | 21. C. E. Pugh |
| 5. C. W. Collins | 22-26. W. K. Sartory |
| 6. J. M. Corum | 27. G. M. Slaughter |
| 7. W. L. Greenstreet | 28. J. E. Smith |
| 8. D. S. Griffith | 29. R. W. Swindeman |
| 9. A. G. Grindell | 30. H. E. Trammell |
| 10. R. C. Gwaltney | 31. M. D. Weaver |
| 11. W. O. Harms | 32. G. T. Yahr |
| 12. W. R. Hendrich | 33. ORNL Patent Office |
| 13. R. L. Huddleston | 34. Central Research Library |
| 14. Y. L. Lin | 35. Document Reference Section |
| 15. S. S. Manson (consultant) | 36-37. Laboratory Records Department |
| 16. W. J. McAfee | 38. Laboratory Records (RC) |
| 17. H. E. McCoy | |

External Distribution

- 39-40. Director, Office of Breeder Technology Projects, Department of Energy, Washington DC 20545
41. Office of Assistant Manager for Energy Research and Development, DOE, ORO, Oak Ridge, TN 37831
- 42-160. Given distribution as shown in DOE/TIC-4500 under categories UC-79T (Liquid Metal Fast Breeder Reactors), UC-79Th (LMFBR - Structural Materials and Design Engineering), UC-79Tk (LMFBR - Components), UC-79Tr (LMFBR - Structural and Component Materials Development)